Examination of the Behaviour of the AUT-to-Reflector VSWR of a Point Source Offset CATR

S.F. Gregson [1,2], S. Pivnenko [3], C.G. Parini [2]
[1] Next Phase Measurements LLC, CA, USA, stuart.gregson@qmul.ac.uk
[2] Queen Mary University London, London, UK
[3] Antenna Systems. Solutions, Santander, Spain

***Abstract*—It is well known that in any reflector antenna, a portion of the wave scattered by the reflector propagates back into the feed horn and manifests itself as a reflected wave at the feed's guided-wave input port. Unlike other sources of mismatch arising within the reflector antenna system, this form of voltage standing wave ratio (VSWR) effect can seldom be compensated for across a reasonable bandwidth by the addition of matching components placed within the guided wave path. What is less broadly understood is that in a Compact Antenna Test Range (CATR) where the test antenna and the parabolic reflector are physically in comparably close proximity to one another, a very similar phenomena can be observed between the reflector and the test antenna, only here, even the opportunity to augment the system with additional matching componentry is unavailable. This paper examines this effect, presenting analytical, computational, and experimental results, that confirm the extent to which this manifests itself within measurements and utilises simple design criteria that can be employed during the development of the CATR folded optics to manage these effects.**

***Index Terms*—CATR, VSWR, standing wave, offset reflector.**

I. INTRODUCTION

In many applications, and especially those concerned with microwave communications, the power reflected back into the feed resulting from scattering from the reflector is of significance as, for example, frequency sensitivity of the input VSWR can cause degradation in wide-band modulated signals. Additionally, for the case of circularly polarised signals involving the use of an orthogonal mode transducer, the wave scattered back into the feed will possess the opposite hand of polarisation, by virtue of the reflection process, to that which was transmitted by the feed, thereby degrading the isolation between the ports. In the asymptotic limit, the magnitude of the voltage-reflector coefficient Γ_R can be estimated using [1],

$$\left|\Gamma_R\right| = G_f \frac{\lambda}{4\pi FL} \tag{1}$$

Here, G_f denotes the peak gain of the feed, FL is the focal length of the parabolic reflector, and λ is wavelength. Related expressions are also developed in [2]. Thus, for typical communication antennas, the voltage-reflector coefficient Γ_R can be above -30 dB, which in many instances is undesirable. One example of a way in which, to some extent, this effect can be managed, is to utilise vertex phase matching, which involves placing a flat plate at the vertex of the reflector with a thickness sufficient to result in a portion of the reflected energy being in antiphase with energy arriving from the remainder of the reflector [3]. However, for the case of a conventional serrated edge compact antenna test range (CATR), as a consequence of the typically very broad frequency band of operation, such cancellation effects are generally unsuccessful; and instead, a virtual vertex design is generally adopted. In this approach, the vertex of the offset paraboloid is located such that it, and its near vicinity, does not fall upon the reflecting portion of the parabolic surface. Unlike the case of the single offset parabolic reflector communications antenna, the situation for the CATR is very different, despite the very obvious similarities between the respective geometries. Here, the test antenna is very nearly as proximal to the reflector as is the feed, which is very definitely not the case for the communication antenna analogue, and so we can expect to experience some similar effects. Furthermore, it is usually desirable to minimise the range length of a given CATR, since this yields a reduction in chamber and absorber cost, which can be quite significant. The down-range position of the QZ is controlled by the need to minimise the likelihood of direct illumination of the QZ by the feed spill-over and to separate the time of arrival in the event of time-gating. However, as the pseudo-plane wave characteristics are generally far more consistent down range than they are across-range, pressure to minimise the distance between the centre of the reflector and the centre of the QZ on the grounds of cost can, if not properly examined, yield sub-optimum CATR designs as this places the AUT in closer proximity to the reflector risking undesirable VSWR related measurement artefacts. Indeed, it has been widely noted that standing wave effects can impact some CATR measurements with errors manifesting themselves on peak gain, EIRP, and near-in sidelobe levels [4].

Although comparatively little attention has been paid to these phenomena within the open literature, many of the general principles have, for some time now, been recognised by the wider community. However, this far more detailed investigation was motivated by a recent query, which necessitated the development of simulation techniques for the estimation of these effects combined with the construction of simple design strategies for their minimisation.

II. CATR Simulation

A detailed description of the current-elements based physical optics CATR simulation technique can be found presented in the open literature, *e.g.* [4], [5], [6], and so because of space constraints, only a summary is presented herein. In a traditional CATR quiet-zone (QZ) prediction, the far-field pattern of the feed antenna is first used to illuminate the offset parabolic reflector surface. The field illuminating the CATR reflector is derived from the assumed known far-field feed pattern where it is assumed that phase centre of the feed is placed at the focal point of the reflector. Here, the inverse radius amplitude term and spherical phase factors are reintroduced into the fields illuminating the reflector. The current elements method can be used to compute the field across the QZ [7]. Here, the fields are replaced with an equivalent surface current density $\underline{J}_s$ which is used as an equivalent source to the original fields. The surface current density across the surface of the reflector can be obtained from the incident magnetic fields and the surface unit normal and is known as the physical-optics approximation [7]. The fields radiated by an infinitesimal electric current element can be obtained from the vector potential & the free-space Green's function using [7, 8],

$$d\underline{H}(P) = \frac{da}{4\pi}\underline{J}_s \times \nabla\psi \qquad (2)$$

Here, the equivalent surface current density is $\underline{J}_s$, da is the elemental surface area, and ψ is the free-space Green's function where the differential operator ∇ only operates on the coordinates of the source point. Lastly, integrating the resulting elemental magnetic field $d\underline{H}$ yields the desired total magnetic field $\underline{H}$. The corresponding elemental electric fields $d\underline{E}$ can be obtained, to a very good approximation, from the elemental magnetic fields $d\underline{H}$ using the far-field TEM condition where again, the field point only need be in the far-field of the *elemental* source which is a requirement that is easily satisfied when the separation is larger than a few wavelengths [4]. In this way the CATR QZ performance may be predicted and, if combined with a reaction integral calculation, simulations of measurements of known AUT and CATR combinations can be obtained [6].

In contrast to the standard CATR modelling approach, in this study the simulations are run in "reverse". Here, we start with the assumed known aperture illumination function for a given test antenna and then use the current elements formulation of equation (2) to compute the fields illuminating the CATR reflector. Thereafter, the conventional physical optics method is used to compute the field scattered back into the CATR QZ as was outlined above. Although computationally intensive, run times are kept to a minimum by virtue of the parallel implementation of the requisite numerical integration, *cf* [9]. In this way, we are able to evaluate the field scattered back into the QZ relative to the radiated field and therefore use this to support the development of efficient design guidelines.

III. CATR Scattering Simulation Results

To illustrate the procedure several simulations were conducted employing different CATR geometries. In each case a 10 GHz, uniformly illuminated, circular aperture AUT, was assumed to be radiating total power of 0 dBm. This was orientated so that its boresight was directed towards the centre of the serrated edge CATR reflector. The geometry of this arrangement can be seen presented in Figure 1. This corresponds to a what we shall call a "standard" configuration. Here, the CATR QZ is denoted by a green sphere, the CATR reflector can be seen to the left of the figure, with the blue cross denoting the vertex (to the left) and the magenta cross denoting the focal point (more central). The magenta lines show rays from the focal point intersecting with the reflector whilst the red rays denote the reflector surface unit normals (*not* the reflected rays), the significance of which will be discussed below.

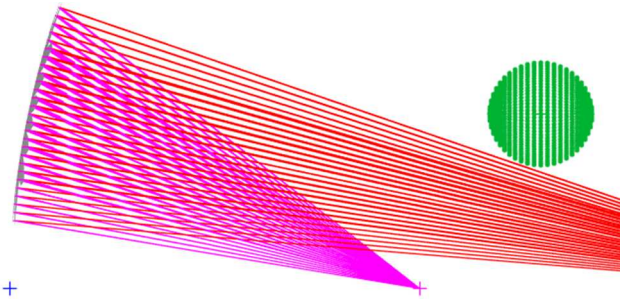

Fig. 1. Geometry of single offset floor-fed CATR shown in side view. "Standard" configuration.

Figure 2a shows the fields illuminating the CATR reflector radiated by the 10 GHz, uniformly illuminated, circular aperture located in the QZ. Here, the total amount of power illuminating the reflector was 0.4 dB less than that which was radiated by the circular aperture test antenna. This is a consequence of the relatively directional character of the antenna. Conversely, Figure 2b shows the field scattered by the CATR reflector which is re-entering the plane of the CATR QZ. Here, the QZ region itself is denoted by the circular white line. From inspection of this figure, it is clear that the amount of field scattered back into the QZ region is comparatively small, with larger field intensities being evident at the bottom of the plot. Here, the total amount of field entering the QZ is -42.3 dB.

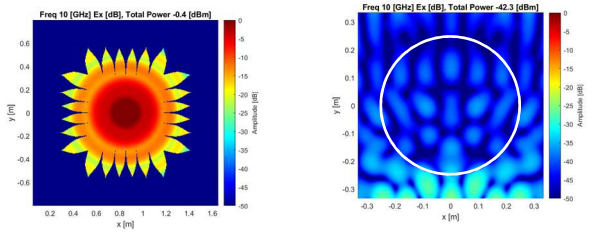

(a) Fields illuminating CATR reflector

(b) Scattered fields illuminating CATR QZ

Fig. 2. False colour plot of fields illuminating CATR reflector and fields scattered back in CATR QZ.

By way of a further illustration two further CATR configurations were examined. These we shall call a "shortened" CATR configuration, and a "short-throw" CATR configuration. These can be seen presented in Figure 3 where the same convention has been adopted as was used in Figure 1 above. In all three cases, QZ diameter, radiated power, frequency, and tip-to-tip CATR reflector size, has been kept consistent, only the focal length and reflector to QZ distances have been allowed to vary.

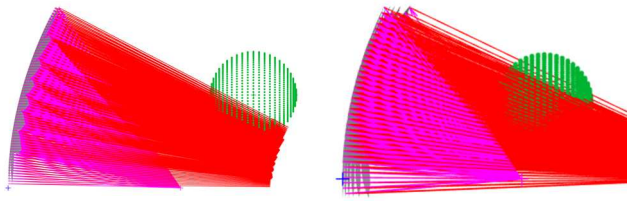

(a) "shortened" floor-fed CATR

(b) "short-throw" corner-fed CATR

Fig. 3. Geometry of single offset CATR shown in side view.

Figure 4a shows the field scattered by the CATR reflector which is re-entering the plane of the CATR QZ (*cf.* CATR configuration shown in Figure 3a). Here, we see there is a greater level of field impinging in the QZ plane and an increase within the QZ itself, as denoted by the dashed blue circle. The total power in the QZ plane has also increased by 9.5 dB to -32.8 dBm. Figure 4b shows equivalent results for the short-throw CATR configuration shown above in Figure 3b which is a corner fed configuration required to realise the reduction in range length. This is the reason the larger scattered field levels are positioned towards the corner of the QZ region.

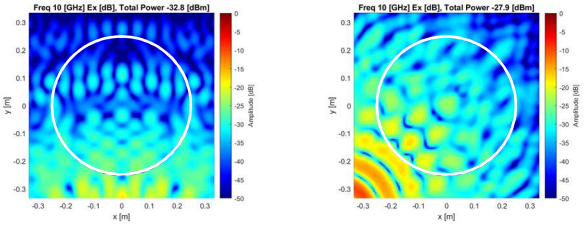

(a) scattered fields illuminating CATR QZ for shortened CATR

(b) scattered fields illuminating CATR QZ for short-throw CATR

Fig. 4. False colour plot of fields scattered back into CATR QZ.

As noted above, the properties of the pseudo plane-wave gradually change as it propagated down range. The results shown in Figures 2b, 4a and 4b therefore represent a snapshot at one location in space. This can be seen illustrated in Figure 5 which shows the amplitude and phase ripple plotted as a function of down range distance for two different example positions in x and y in the QZ for the short-throw corner fed CATR configuration. Here, we see that the amplitude of ripple of the cuts in the corner of the QZ (Figures 5a, 5b) are larger than when located more centrally (Figures 5c, 5d) which aligns with the character of the plots shown in Figure 4b. However, these represent just two example positions and changing the position of the down-range cuts in (x, y) will result in cuts with differing amplitude ripples. Thus, as in reality the QZ is a volume of space, it is preferable to aggregate the scattering effects across this region of space. This can be accomplished by presenting the amplitude and phase differences statistically in the form of a cumulative distribution function (CDF) plot [10] of the amplitude and phase differences. In this way we can derive a more statistically significant assessment of the respective scattering performance of the three candidate CATR configurations.

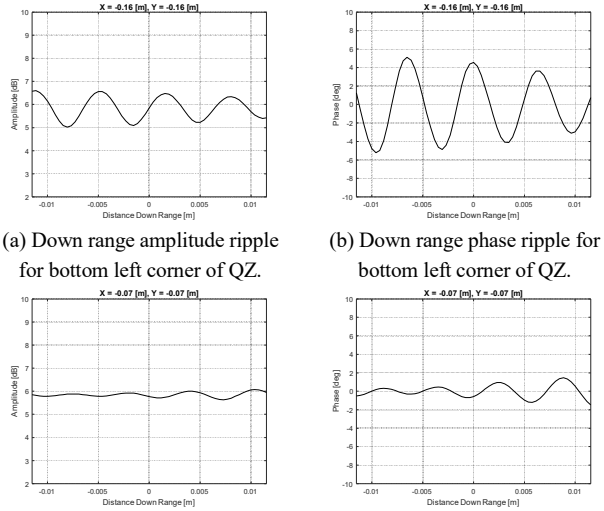

(a) Down range amplitude ripple for bottom left corner of QZ.

(b) Down range phase ripple for bottom left corner of QZ.

(c) Down range amplitude ripple for more central region of QZ

(d) Down range phase ripple for more central region of QZ

Fig. 5. Down range amplitude and phase ripples in different places in QZ.

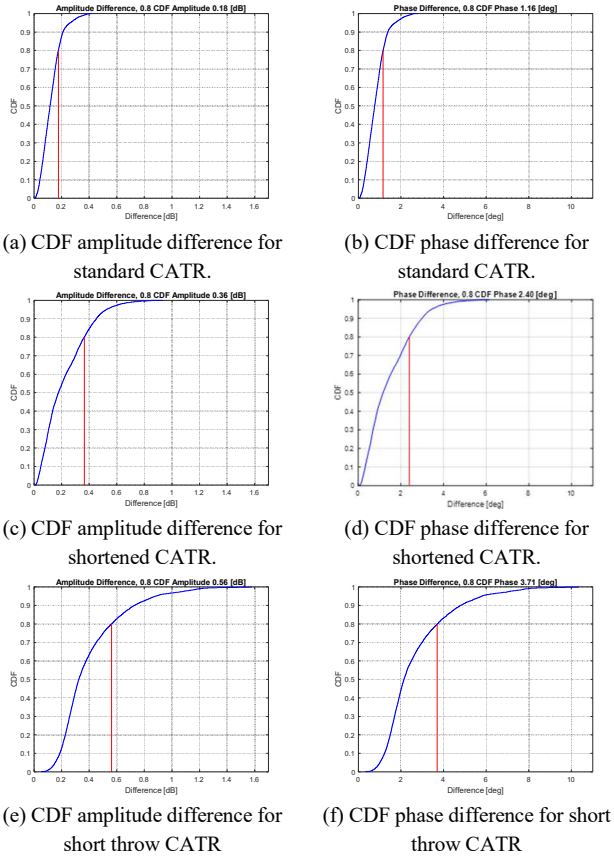

(a) CDF amplitude difference for standard CATR.

(b) CDF phase difference for standard CATR.

(c) CDF amplitude difference for shortened CATR.

(d) CDF phase difference for shortened CATR.

(e) CDF amplitude difference for short throw CATR

(f) CDF phase difference for short throw CATR

Fig. 6. CDF plots of the amplitude and phase.

Figure 6a presents the CDF plot for the amplitude ripple aggregated over the QZ region for the standard configuration. Here, the 0.8 CDF level is highlighted where we can see that 80% of the amplitude differences were less than 0.18 dB. The benefit of the CDF approach is that if another level is desired, *e.g.* 1σ, 2σ, *etc*. this can be easily read from the plot. Figure 6b presents an equivalent plot for the phase difference where at the 0.8 CDF level the phase difference is 1.16 deg. Inspection of Figure 6a-f reaffirms the general observations noted above. Here, we see that for a CDF of 0.8 the amplitude difference is 0.18 dB for the standard CATR case, 0.36 dB for the shortened CATR case, and 0.56 dB for the short-throw CATR case. Similarly, for a CDF of 0.8 the phase difference is 1.16° for the standard CATR case, 2.4° for the shortened CATR case, and 3.71° for the short-throw CATR case.

IV. VSWR Implications for CATR Design

In general, the parabolic reflector tends to redirect the field incident on the reflector towards the CATR feed. This is especially true for the case considered here where the boresight direction of the AUT is on the range *z*-axis. However, in Figures 4a and 4b, we clearly see that due to close position of the QZ to the reflector, some of the field is scattered back into the QZ, noticeably increasing the amplitude and phase ripples.

It can be observed that the region where the intensity of this scattered field is greatest coincides with those regions where we see the reflector surface normals (depicted by the red rays) passing through the QZ, as shown in Figure 1 and Figure 3a and Figure 3b. This suggests that these simple diagrams can be used as an aid to the CATR designer providing rapid feedback on the likely test antenna to reflector VSWR behaviour without the need for time consuming and computationally intensive electromagnetic simulations.

V. Measured Results

Experimental validation of the observed effects was carried out by measuring the VSWR in an installed CATR with QZ size of 0.6m of a "standard" configuration. This CATR is side-fed just below horizontal on the right side looking towards the reflector and so stronger VSWR effects would be expected on the right side of the CATR QZ in line with the results for the opposite configuration shown in Figure 4b above. In this setup, the Antenna Under Test (AUT) positioner is installed on a longitudinal slide allowing to change the distance between the AUT positioner and reflector. A Field Probe Scanner holding a Standard Gain Horn (SGH) was mounted onto the AUT positioner and measurements of the VSWR was carried out while moving the SGH transversally through the QZ at several distances from the reflector. Measured variations of the VSWR amplitude and phase at 10.2 GHz are shown in Figure 7. It can be seen that in the nominal centre of the QZ, smooth and slow variations are present, arising likely due to small changes in the RF cable shape.

On the other hand, in the position closer to the reflector, stronger fast varying ripples are observed on the right side, towards the feed, where interaction of the SGH with the reflector is expected. It is noted that in this experiment, the feed was dismounted, and its positioner was covered with absorbers. Thus, the only interactions present are between the SGH and the reflector.

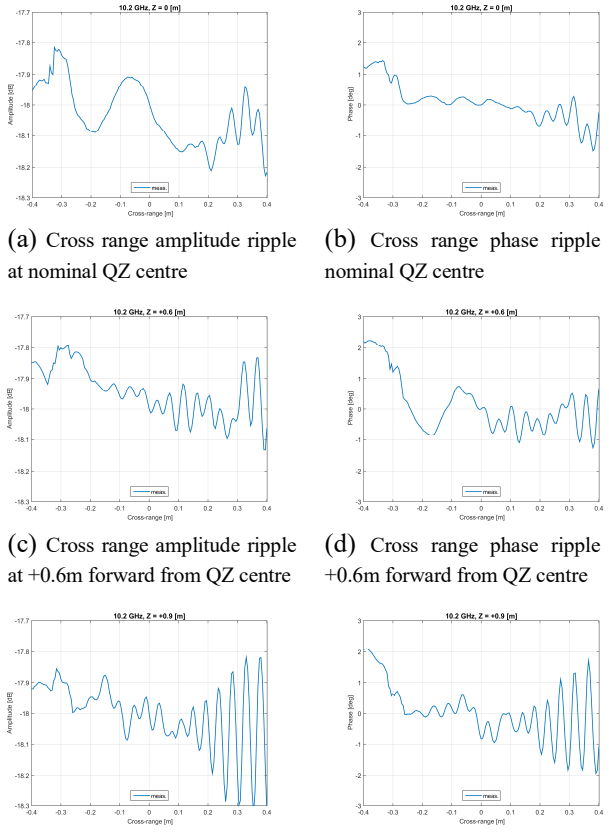

(a) Cross range amplitude ripple at nominal QZ centre

(b) Cross range phase ripple at nominal QZ centre

(c) Cross range amplitude ripple at +0.6m forward from QZ centre

(d) Cross range phase ripple at +0.6m forward from QZ centre

(e) Cross range amplitude ripple at +0.9m forward from QZ centre

(f) Cross range phase ripple at +0.9m forward from QZ centre

Fig. 7. Measured cross range VSWR.

In addition, several longitudinal scans were carried out with the SGH located on the left and right side at the edges of the QZ. The results are shown in Figure 8. The nominal QZ position in this scale is between [-0.3, 0.3] m, with positive values being closer to the CATR reflector. These results are affected by poor signal stability due to moving and flexing the RF cable. Several spikes can be observed, which appear most likely due to rapid changes in the RF cable shape. Nevertheless, it can well be seen that on the left side of the QZ, the ripples remain relatively small, while on the right side of the QZ, ripples are a bit stronger already in the front part of the QZ and become much larger closer to the reflector.

Noticeable increase of the ripples in the front part of the QZ, Figure 8c-d, around the down range location [+0.1, +0.2] may be caused by relatively large SGH aperture intercepting scattering from the serrations, which are rather long in this particular CATR setup.

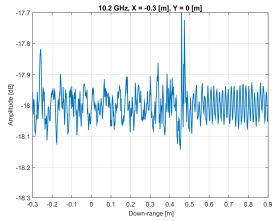

(a) Down range amplitude ripple, left side of the QZ

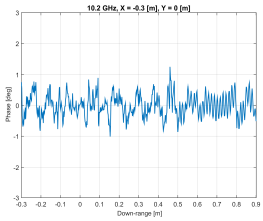

(b) Down range phase ripple, left side of the QZ

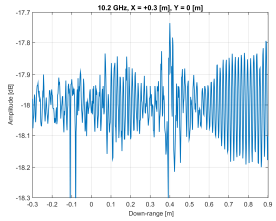

(c) Down range amplitude ripple, right side of the QZ

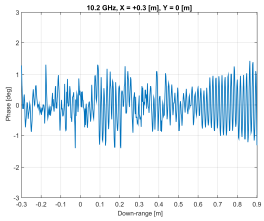

(d) Down range phase ripple, right side of the QZ

Fig. 8. Measured down range VSWR between standard gain horn as AUT and the CATR reflector.

VI. Summary and Conclusion

This paper summarises a long-term study into reflector VSWR for single offset reflector, serrated edge, compact antenna test ranges that highlights potential VSWR effects that can exist between the test antenna and the range reflector. Standing wave effects are well-known and can, for example, be seen to degrade the accuracy of gain, equivalent isotropic radiated power (EIRP), and near-in sidelobe level measurements in some CATR measurements. This paper examines this effect in far greater detail than has previously been the case, presenting electromagnetic simulations showing the relative fields scattered back into the region of space where the test antenna is located. Cumulative distribution function plots are utilised to present a summary of the relative effects throughout the region of space where the test antenna is positioned. It is then shown that the regions of greatest scattered fields correspond to regions where we see CATR reflector unit surface normal vectors piercing this portion of space. The ability to use this form of visual design tool to provide convenient, rapid, methods for the optimisation of new serrated edge single offset reflector CATR designs is expounded. Although as a consequence of space, only a medium gain antenna example is illustrated within the simulations, similar effects were observed for the case of a low gain radiator of only a few wavelengths in size. Crucially, the validity of the predictions of the numerical electromagnetic simulations were verified and confirmed by results of an extensive experimental campaign that involved measuring variations of the VSWR amplitude and phase at 10.2 GHz within a candidate CATR. These measurements confirmed that for the CATR system considered, reflector VSWR effects were very small but that if the AUT were to be displaced towards the reflector the predicted effects could be seen. This confirmed both the modelling and the CATR design rules that have been developed.

As this paper recounts the results of an ongoing study, the future work is to include conducting a similar examination of the behaviour of blended rolled edge CATRs, as the design guides developed herein suggest that by virtue of the blended rolled reflector edge treatment, it is possible that the effects observed here may well become more pronounced in that case.

References

[1] S. Silver, “Microwave Antenna Theory and Design”, McGraw-Hill, 1949, Dover Publications, New York, 1965, 65-22730.

[2] G.T. Poulton, S.H. Lim, “Calculation of Input-Voltage Standing Wave Ratio for a Reflector Antenna”, Electronic Letters, 1972, 8, 99. 610-611.

[3] G.T. Poulton, T. Almoayyed, “Optimum Vertex Plate Design for Reflector Antennas”, European Microwave Conference, 1973, paper C.4.4.

[4] C.G. Parini, S.F. Gregson, J. McCormick, D. Janse van Rensburg, T. Eibert, “Theory and Practice of Modern Antenna Range Measurements 2nd Expanded Edition”, IET Electromagnetic Waves series 55 ISBN 978-1-83953-126-2, 2021.

[5] C.G. Parini, R. Dubrovka, S.F. Gregson, “Compact Range Quiet Zone Modelling: Quantitative Assessment using a Variety of Electromagnetic Simulation Methods”, LAPC, November 2015.

[6] C.G. Parini, R. Dubrovka, S.F. Gregson, “CATR Quiet Zone Modelling and the Prediction of 'Measured' Radiation Pattern Errors: Comparison using a Variety of Electromagnetic Simulation Methods” AMTA October 2015.

[7] A.W. Rudge, K. Milne, A.D. Olver, P. Knight, “The Handbook of Antenna Design Volume I”, IEE Press, 1982.

[8] G.L. James, “Geometrical Theory of Diffraction for Electromagnetic Waves”, 3rd Edition, IET Press, 2007.

[9] M. Dirix, S.F. Gregson, "Optimisation of the Serration Outline Shape of a Single Offset-Fed Compact Antenna Test Range Reflector Using a Genetic Evolution of the Superformula", EuCAP, Düsseldorf, Germany, March 2021.

[10] S.F. Gregson, Z. Qin, C.G. Parini, “Compressive Sensing in Massive MIMO Array Testing: A Practical Guide”, IEEE Transactions on Antennas and Propagation, vol. 70, no. 9, pp. 7978-7988, Sept. 2022.